



Research Article

Hybrid gel composites of melanin and tungsten oxide nanoparticles for enhanced electromagnetic radiation attenuation

Saad Aldawood^{a,*}, Khalid E. Alzahrani^a, Ahmad A. Alsaleh^b, Sayed M. Ali^a, Aziz A. Aziz^a, A. M. Kamal^a, Hamoud Kassim^a

^aDepartment of Physics and Astronomy, King Saud University, College of Science, Department of Physics, 11451, Riyadh, Saudi Arabia

^bDepartment of Chemistry, King Saud University, College of Science, Department of Physics, 11451, Riyadh, Saudi Arabia

ARTICLE INFO

Keywords:

Linear attenuation coefficient
Melanin-based composites
Polymer nanocomposites
Radiation shielding
WO₃ nanoparticles

ABSTRACT

Polymer-based composites containing nanostructured tungsten oxide (WO₃) within a Pluronic P123-melanin matrix (PM) were prepared and evaluated for high-energy electromagnetic radiation shielding. Composites containing 5%, 10%, 15%, and 20% WO₃ by weight were structurally and optically characterized. X-ray diffraction (XRD) validated the crystalline structure of WO₃, while scanning electron microscopy (SEM) and energy-dispersive X-ray spectroscopy (EDS) revealed uniformly distributed plate-like nanostructures. UV-Vis and photoluminescence (PL) analyses proved significant UV absorption and adjustable emission correlated with increasing WO₃ concentration. Fourier-transform infrared (FTIR) spectroscopy confirmed the chemical stability of the polymer-melanin framework. The addition of WO₃ nanoparticles significantly enhanced the radiation shielding performance, with the 20% WO₃ composite exhibiting the most effective attenuation. Both the linear attenuation coefficient (LAC) and mass attenuation coefficient (MAC) increased with WO₃ concentration, particularly at photon energies below 200 keV. The mean free path (MFP) of WO₃-NPs/PM-5 decreases from 0.275, 6.02, and 7.97 cm to 0.133, 2.85, and 4.13 cm in WO₃-NPs/PM-20 at 31, 662, and 1332 keV, and the half value layer (HVL) of WO₃-NPs/PM-5 decreases from 0.39, 8.69, and 11.05 cm to 0.19, 4.11, and 5.96 cm in WO₃-NPs/PM-20 at 31, 662 and 1332 keV. This reduction across all photon energies is attributed to the increasing concentrations of nanoparticles.

1. Introduction

Electromagnetic radiation (EMR) shielding is crucial for ensuring healthy well-being as well as protecting electronic equipment, which led to prompting investigations into lightweight, flexible, and eco-friendly composite materials as alternatives for conventional metal-based shields (Fionov *et al.*, 2022) (Omana *et al.*, 2022). Polyaniline (PANI), polypyrrole, polythiophene, and other conducting polymers, as well as hybrid fillers and MXene-based systems, have promise for electromagnetic interference (EMI) shielding (Shahapurkar *et al.*, 2022a, Omana *et al.*, 2022). These materials can be engineered to exhibit tunable dielectric and magnetic properties, leading to improved electromagnetic absorption with minimal reflection (Sastri *et al.*, 2018).

Electrospun polycaprolactone fibers containing 80 wt% tungsten exhibited effective radiation shielding features. *In vivo* X-ray inspections revealed a 1.5-fold decrease in radiation-induced apoptosis when utilizing a 24-layer barrier in comparison to unshielded exposure (Giuliani *et al.*, 2024). Particular attention was directed towards conducting polymers such as polyaniline, polypyrrole, and polythiophene, which are regarded as effective shielding materials (Shahapurkar *et al.*, 2022b). The advancement of polymeric nanocomposites for electromagnetic

shielding emphasizes materials engineered with specific dielectric and magnetic characteristics. These properties are optimized for efficient microwave absorption and minimal reflection. This approach emphasizes multilayer designs that provide adjustable electromagnetic responses (Fionov *et al.*, 2022). A correlation was established between EMI shielding effectiveness, electrical conductivity, and thickness in polymer composites, without regard to filler type. This relationship, supported by experimental and literature data, promotes accurate predictions of shielding performance without direct measurement (Retailleau *et al.*, 2022).

Nanostructured tungsten oxide (WO₃) has emerged as a highly effective material for EMR shielding due to its exceptional dielectric properties and high density (Retailleau *et al.*, 2022; Solak *et al.*, 2024). The nanoscale structure and enhanced interfacial contacts considerably enhance electromagnetic absorption and attenuation, thereby reducing radiation risk in electronic and communication systems (Shaaban *et al.*, 2024; Alsaif *et al.*, 2024; Sood *et al.*, 2024). Furthermore, WO₃ offers chemical stability, environmental safety, and adjustable optical properties, positioning it as a promising candidate for advanced EMI protection applications (Yao *et al.*, 2021; Khan *et al.*, 2024; Kahraman *et al.*, 2025; Zhou *et al.*, 2024).

*Corresponding author:

E-mail address: sdawood@ksu.edu.sa (Saad Aldawood)

Received: 06 October, 2025 Accepted: 12 December, 2025 Epub Ahead of Print: 09 February, 2026 Published: 24 February, 2026

DOI: 10.25259/JKSUS_1568_2025

Recent advancements in polymer nanocomposites for EMI shielding, particularly those incorporating hybrid fillers and MXenes, highlight the influence of microstructure and filler type on shielding effectiveness. These developments also emphasize the importance of synthesis methods and mechanical properties. (Omana et al., 2022). PANI ferrite nanocomposites exhibit adjustable, multifunctional characteristics with improved EMI shielding. Notably, decreasing ferrite particle size to below 30 nm markedly enhances superparamagnetic behavior and shielding efficacy. (Rayar et al., 2023). Polyethylene (PE) nanocomposites incorporating tungsten-decorated boron nitride nanosheets (W-BNNS) were synthesized, resulting in a uniform distribution of tungsten that inhibited the restacking of BNNS and the aggregation of nanoparticles. The composites showed mechanical strength, electrical conductivity, and enhanced shielding against neutron and gamma radiation (Kim et al., 2022). Structural asymmetry and tailored conductive networks were developed in composites to improve electromagnetic absorption and shielding. It consists of a foam absorption layer and an AgP shielding layer, achieving an effectiveness of 70 dB, an absorption coefficient of 0.86, and enhanced thermal and mechanical stability (Li et al., 2023). Lightweight recycled linear low-density polyethylene (LLDPE) composites reinforced with up to 70% tungsten exhibited optimal density and radiation shielding at maximum loading, as confirmed by LAC, HVL, and MFP measurements, alongside low porosity ($\leq 7\%$) and relative densities ranging from 93.3% to 97.7%. (Rotkovich et al., 2024).

Melanin, a naturally occurring biopolymer, has demonstrated intrinsic photoprotective capabilities, particularly against UV radiation. Its unique mechanism allows rapid dissipation of high-energy photons as heat through excited-state relaxation and partial proton transfer. Beyond UV, melanin interacts with X-rays and gamma rays, broadening its potential applications in biomedical and shielding technologies (Xie et al., 2024). Melanin nanoparticles have been investigated for use in cosmetics due to their natural photoprotection and pigmentation properties (Menichetti et al., 2024). However, the photoprotective efficacy of melanin depends on its distribution within the epidermis. Studies using reconstructed human epidermis models have shown that uneven melanin distribution and lack of perinuclear melanin localization may compromise UV protection and elevate the risk of DNA damage in keratinocytes (Zamudio Díaz et al., 2024). Nonetheless, melanin's ability to absorb and dissipate harmful UV radiation contributes to reduced DNA damage and decreased skin cancer risk (Xie et al., 2024; Zamudio Díaz et al.; 2024, El-Zawawy et al., 2024).

Pluronic P123-melanin matrix reinforced with gel-like WO_3 nanostructures offers UV blocking and significantly improved gamma shielding, as demonstrated by the highest LAC/MAC enhancements and reduced MFP/HVL at sub-200 keV. This study aims to synthesize and characterize a novel polymer-based gel composite incorporating melanin and tungsten oxide nanoparticles for enhanced electromagnetic radiation shielding efficiency.

2. Materials and Methods

2.1 Preparation of WO_3 -NPs/PM composites

A solution of Pluronic P123-Melanin (PM) was prepared by dissolving Pluronic P123 in deionized water at concentrations ranging between 15% and 30% (w/v). Separately, a melanin solution was prepared by dissolving 1.0 g of melanin in 1.0 L of deionized water with continuous stirring to ensure complete dispersion. The melanin solution was subsequently added dropwise to the Pluronic P123 solution while maintaining continuous stirring to ensure uniform mixing. The temperature was incrementally raised to 35–40 °C during the addition process to ensure adequate homogenization of the components.

Commercial nanostructured tungsten oxide powder (Millipore-Sigma, St. Louis, MO, USA) was subsequently added to the prepared PM solution at varying weight ratios of 5%, 10%, 15%, and 20% relative to the total solution weight. The resulting mixtures were stirred continuously to ensure uniform dispersion of the tungsten oxide nanoparticles within the Pluronic P123-Melanin matrix. To prevent the agglomeration of nanoparticles, the mixture underwent sonication for 1 h. The composite solutions were labelled as WO_3 -NPs/PM-x, with x

being the weight fraction of nanostructured tungsten oxide in the PM solution. The synthesized WO_3 -NPs/PM composites first displayed a viscous colloidal liquid form immediately after mixing. The samples were allowed to dry under ambient conditions for almost 10 days, resulting in a dense, gel-like consistency.

2.2 Gamma ray shielding measurement setup

The gamma shielding performance of the synthesized composites was evaluated using a NaI(Tl) scintillation detector (BICRON 2M2/2; crystal size: 2" \times 2"), coupled with a CAEN N6730B digitizer. The measurements employed point radioactive sources including Am-241 (178,222 Bq; 31 and 59.5 keV), Ba-133 (9,324 Bq; 81, 303, and 356 keV), Cs-137 (1.14×10^5 Bq; 662 keV), and Co-60 (23,643 Bq; 1173 and 1332 keV). During the experiment, the shielding samples were placed 5 cm from the gamma source and positioned between the source and the detector, which was fixed at 15 cm from the source. Radiation counts were recorded over 30-min intervals, with each measurement repeated three times to ensure reproducibility. The mean values were calculated and used for subsequent analysis of linear attenuation coefficient (LAC), mass attenuation coefficient (MAC), half-value layer (HVL), and mean free path (MFP).

3. Result and Discussion

The synthesized WO_3 -NPs/PM composites initially resulted in viscous colloidal solutions, which subsequently dried into dense, gel-like materials over a period of 10 days at room temperature. This final state restricted the use of conventional structural methods such as X-ray diffraction (XRD), scanning electron microscopy (SEM), and energy-dispersive spectroscopy (EDS), which were only conducted on tungsten oxide and melanin samples separately devoid of Pluronic P123 (WO_3 -NPs/M).

3.1 XRD patterns of the composites

The XRD patterns of the WO_3 -NPs/PM composites (Fig. 1) exhibit prominent diffraction peaks at $2\theta \approx 23.1^\circ$ (002), 23.6° (020), 24.3° (022), 33.6° (222), 49.8° (400), and 55.7° (420), which correspond to the crystalline planes of monoclinic WO_3 , consistent with JCPDS card No. [83-0950]. These results confirm that the crystalline structure of WO_3 nanoparticles is retained after incorporation into the Pluronic-melanin matrix. No additional peaks were observed, indicating phase purity and the absence of crystalline by-products.

Using the Debye-Scherrer equation, the average crystallite size of the WO_3 nanoparticles was calculated to be [169.84] nm, suggesting nanocrystalline dimensions favorable for electromagnetic interaction. No significant peak shift or broadening was detected, indicating minimal lattice strain from matrix interaction. The retention of crystallinity is crucial for effective radiation shielding, as it directly influences the electronic density and interaction probability with incoming photons.

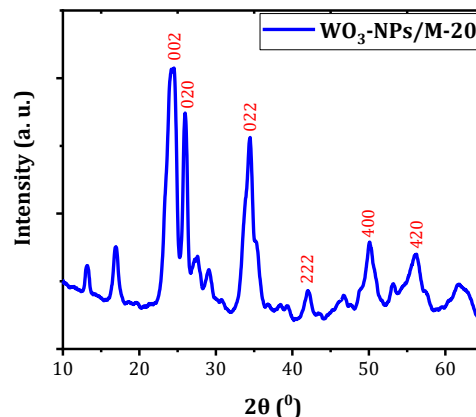


Fig. 1. XRD patterns of WO_3 nanoparticles (WO_3 -NPs/M).

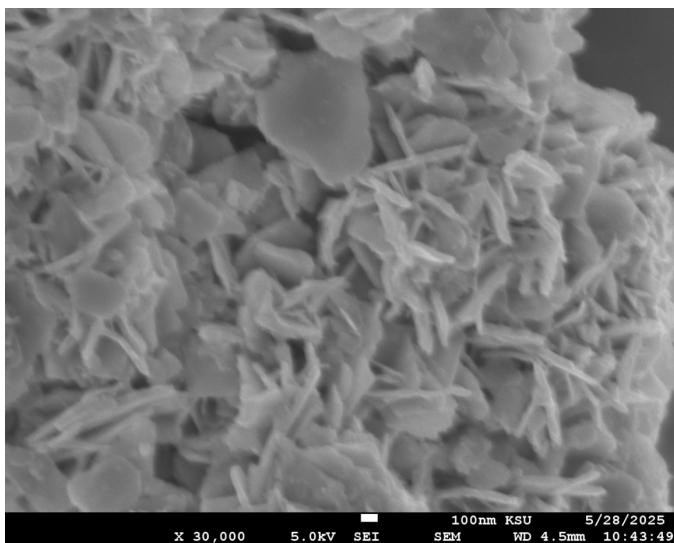


Fig. 2. SEM image of tungsten trioxide (WO_3) nanoparticles dispersed in melanin WO_3 -NPs/M. The image was captured at a magnification of 50,000x with a scale bar of 100 nm.

3.2 Scanning electron microscopy

The SEM micrographs presented in Fig. 2 illustrate the surface morphology of WO_3 -NPs/M composite at a magnification of 50,000x. The nanoparticles display primarily plate-like to rod-like nanostructures. The composite nanostructures exhibit lateral sizes generally between about 100 nm and 300 nm, with the presence of some smaller fragments noted, suggesting some degree of agglomeration or partial fragmentation. The observed plate thicknesses appear to be below 50 nm, indicating the formation of ultrathin nanostructures. This nanoscale morphology is expected to enhance surface area and interaction with the polymer-melanin matrix, potentially improving the composite's radiation shielding performance.

3.3 Elemental composition and surface analysis via EDX spectroscopy

Fig. 3 presents the SEM micrograph and the corresponding EDS analysis of the WO_3 -NPs/PM-20 composite. The SEM image displays a textured, clustered surface morphology characterized by plate-like nanostructures, indicative of effective nanoparticle dispersion. The EDS spectrum confirms the presence of tungsten (W), oxygen (O), and carbon (C), which are consistent with the expected components of WO_3 nanoparticles and the Pluronic-melanin (PM) matrix. Quantitative analysis indicates tungsten constitutes 70.33 wt%, oxygen 19.43 wt%, and carbon 10.25 wt%. The significant tungsten signal verifies the prevalent existence of WO_3 nanoparticles in the examined area,

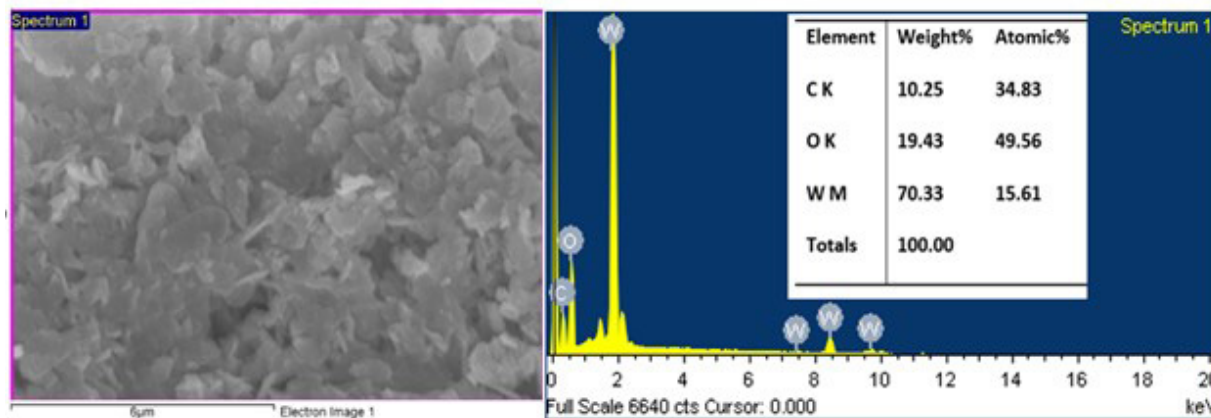


Fig. 3. The SEM image and corresponding EDX spectrum of the WO_3 -NPs/PM-20 composite, confirming the elemental composition and uniform dispersion of WO_3 nanoparticles within the pluronic-melanin matrix.

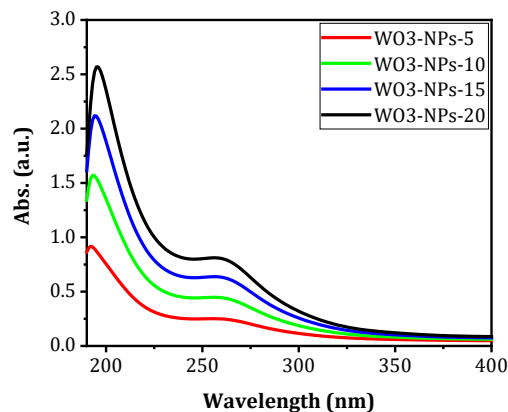


Fig. 4. UV-Vis absorption spectra of WO_3 -NPs with varying WO_3 nanoparticle concentrations.

whereas the contributions from carbon and oxygen mainly stem from the polymer and melanin elements. The results confirm the effective integration and surface distribution of WO_3 within the composite.

3.4 UV-Vis absorption spectroscopy

Fig. 4 presents UV-Vis absorption spectra of WO_3 -NPs composite solutions with varying tungsten oxide nanoparticle loadings: 5%, 10%, 15%, and 20% by weight. All samples exhibit a prominent absorption band in the UV region (approximately 190-200 nm) and additional absorption at 250-275 nm. As the WO_3 content increases, a slight enhancement in absorbance intensity is observed across the spectrum, particularly in the UV region.

3.5 Photoluminescence spectroscopy analysis

Fig. 5 presents the photoluminescence (PL) spectra of WO_3 -NPs composites, excited at 225 nm, with varying WO_3 nanoparticle loadings (5%, 10%, 15%, and 20% by weight). The spectra exhibit distinct emission peaks at approximately 410 nm. A clear concentration-dependent enhancement in PL intensity is observed, with the WO_3 -NPs-20 sample showing the highest emission and WO_3 -NPs/PM-5 the lowest. This trend confirms that the photoluminescence properties of the composites can be effectively tuned by varying the WO_3 nanoparticle content, potentially impacting their optoelectronic performance.

3.6 FTIR analysis

Fig. 6 shows the Fourier transform infrared (FTIR) transmittance spectra of WO_3 -NPs/PM composites with varying tungsten oxide nanoparticle loadings (5%, 10%, 15%, and 20% by weight). All spectra

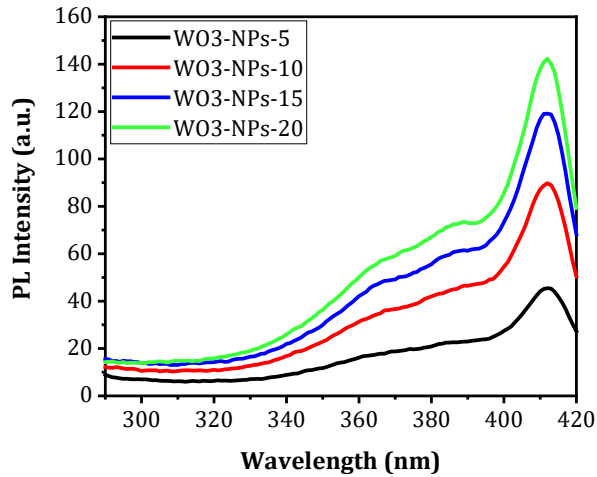


Fig. 5. PL spectra of WO_3 -NPs, excited at 225 nm, with varying WO_3 nanoparticle concentrations (5–20 wt%).

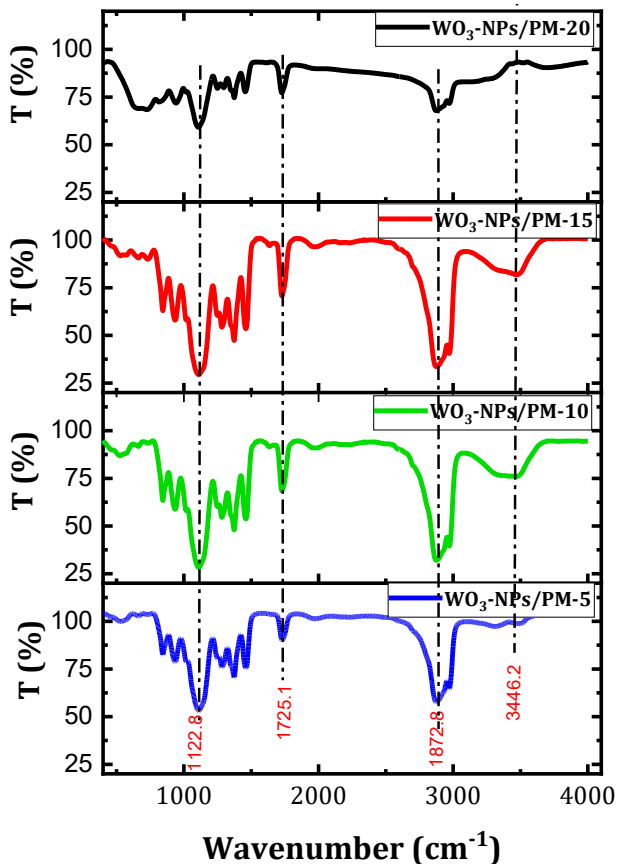


Fig. 6. FTIR transmittance spectra of WO_3 -NPs/PM composites containing 5%, 10%, 15%, and 20% tungsten oxide nanoparticles by weight, illustrating the influence of increasing WO_3 content on vibrational band intensities within the polymer–melanin matrix.

exhibit characteristic absorption bands corresponding to functional groups present in the Pluronic P123–melanin (PM) matrix. Prominent peaks are observed around 1122.8 cm^{-1} (C–O–C stretching of Pluronic P123), 1725.1 cm^{-1} (C=O stretching likely from the melanin or polymer matrix), 1872.8 cm^{-1} (possible overtone or combination bands), and 3446.2 cm^{-1} (O–H stretching of water or surface hydroxyl groups).

As the WO_3 nanoparticle content increases, a systematic decrease in transmittance intensity is observed across all bands, with the WO_3 -NPs/PM-20 sample showing the most pronounced attenuation. This

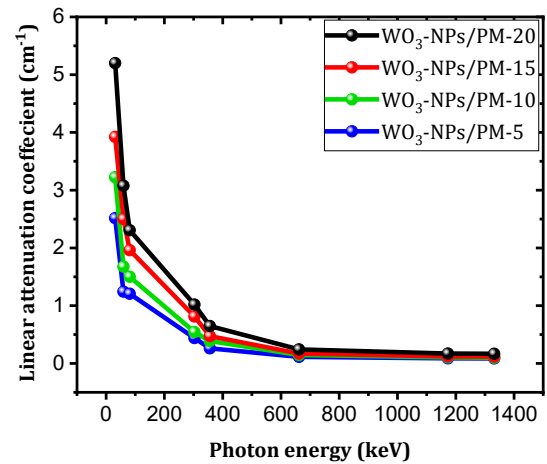


Fig. 7. LAC as a function of photon energy for WO_3 -NPs/PM composites with varying tungsten oxide nanoparticle loadings (5%, 10%, 15%, and 20% by weight).

behavior suggests increased absorption and possible scattering effects due to the higher nanoparticle density, which may partially obscure the vibrational signals of the organic matrix. Importantly, the consistent positions of the characteristic peaks across all samples indicate that the incorporation of WO_3 does not significantly alter the chemical structure of the PM composite. Rather, the spectral changes are predominantly physical in nature, associated with increased optical density and potential particle–matrix interactions.

The FTIR spectra of the composites (WO_3 -NPs/PM-10, WO_3 -NPs/PM-10, WO_3 -NPs/PM-15, and WO_3 -NPs/PM-20) are consistent. Consequently, it was determined that the inclusion of the filler did not affect the functional group intensity of the polymer, as no chemical interaction was observed between the polymer and WO_3 , indicating that only physical interaction took place.

3.7 Radiation attenuation performance

Fig. 7 presents the variation of the LAC (cm^{-1}) as a function of photon energy (keV) for tungsten trioxide nanoparticles (WO_3 -NPs) dispersed in a polymer matrix at different weight fractions: 10%, 20%, 30%, and 40% (denoted as WO_3 -NPs/PM-5, WO_3 -NPs/PM-10, WO_3 -NPs/P-15, and WO_3 -NPs/P-20, respectively). The data show a significant decrease in the LAC as photon energy increases, particularly in the low-energy range (0–200 keV), where the photoelectric absorption is dominant. Higher WO_3 content corresponds to enhanced attenuation across all energy levels, with the WO_3 -NPs/PM-20 composite demonstrating the highest LAC values. This trend highlights the role of WO_3 nanoparticles in improving photon interaction and shielding efficiency, especially at lower energies. At higher photon energies, the differences among the samples diminish, reflecting the reduced influence of material composition on photon attenuation in this range.

Fig. 8 presents the MAC of WO_3 -NPs/PM composites as a function of photon energy for polymer composites reinforced with different weight percentages of tungsten oxide nanoparticles (WO_3 -NPs): 5, 10, 15, and 20 wt%. Across all samples, the MAC decreases with increasing photon energy, which is consistent with the general behavior of photon interaction with matter, wherein lower-energy photons are more readily absorbed. Attenuation is most effective in the low-energy region (below 200 keV), where the photoelectric absorption mechanism dominates. At higher energies, particularly beyond 500 keV, the attenuation performance significantly declines due to the reduced probability of photoelectric interactions and the increased dominance of Compton scattering. The data clearly show that composites with higher WO_3 -NP content exhibit superior radiation shielding across the entire energy spectrum, with the WO_3 -NPs/P-20 sample consistently achieving the highest MAC values. This improvement is attributed to the high atomic number and density of tungsten, which enhances photon attenuation through both photoelectric absorption and scattering processes (Sayyed et al., 2024; Hsieh and Taguchi, 2024; Almousa et al., 2024; Khattari,

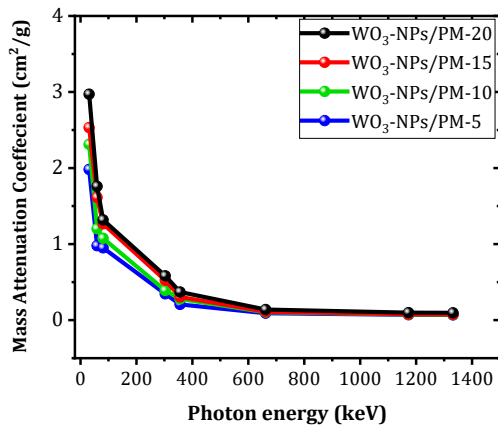


Fig. 8. MAC vs. photon energy for WO₃-NPs/PM composites with varying tungsten oxide nanoparticle concentrations (5%, 10%, 15%, and 20% by weight).

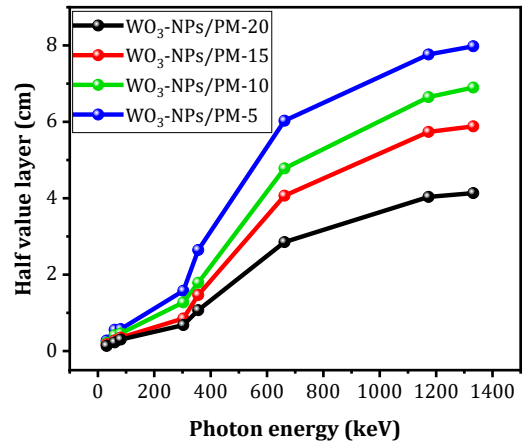


Fig. 9. HVL as a function of photon energy for WO₃-NPs/PM composites with varying concentrations.

Table 1. Comparison of MAC at 662 keV between WO₃-NPs/PM composites and conventional shielding materials.

	Sample	Energy (662 keV)	Study
MAC (cm ² /g)	WO ₃ -NPs/PM-5	0.090	Present
	WO ₃ -NPs/PM-10	0.103	
	WO ₃ -NPs/PM-15	0.109	
	WO ₃ -NPs/PM-20	0.138	
	Lead	0.100	(Eren Belgin et al., 2015)
	Tungsten carbide	0.09	(Jamal AbuAlRoos et al., 2020)
	Lead	0.129	
	Tungsten-Fiber	0.08	(Hou et al., 2018)
	Zirconium	0.057	(Abbasova et al., 2019)
	Composite (Ba, Al, Si)	0.084	

2025). The results confirm that increasing the concentration of WO₃ nanoparticles substantially improves the shielding efficiency of the composites, particularly at lower photon energies, making them suitable candidates for radiation protection applications in medical, industrial, and electronic fields (Al-Ghamdi et al., 2022; Hannachi et al., 2023).

Table 1 presents a comparison of the MAC values obtained from the fabricated composites with those of the conventional shield reported at 662 keV. We select 662 keV as a reference energy for comparison because it is linked to the distinct gamma emission from Cesium-137 (Cs-137), a commonly utilized and readily available radioactive isotope.

Fig. 9 illustrates the inverse relationship between the tungsten oxide (WO₃) content and the HVL in WO₃-NPs/PM composites as a function of photon energy. HVL, which represents the thickness of material required to reduce the intensity of incident radiation by 50%, is a critical parameter for assessing shielding effectiveness (Sayyed et al., 2022; Al-Hadeethi et al., 2020). HVL increases with increasing photon energy, indicating that higher-energy photons penetrate deeper into the material and require greater thickness for effective attenuation. The composites with higher WO₃ nanoparticle loading (WO₃-NPs/PM-20 and WO₃-NPs/PM-15) consistently demonstrate lower HVL values, reflecting superior radiation attenuation capability. This is attributed to the high atomic number and density of tungsten, which significantly enhances photon interaction probabilities, especially via photoelectric absorption and Compton scattering at lower and intermediate energies (Sartoretti et al., 2024). The separation between the HVL curves becomes more pronounced at photon energies below approximately 600 keV, where the influence of WO₃ loading is most significant. At higher photon energies (above ~1000 keV), the HVL curves tend to converge slightly, suggesting that the relative difference in attenuation performance between samples diminishes, as high-energy photons

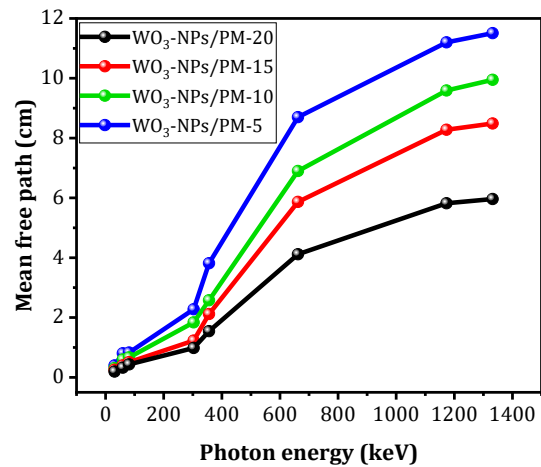


Fig. 10. Mean free path (MFP) as a function of photon energy for WO₃-NPs/PM composites with varying WO₃ nanoparticle loadings.

primarily interact through pair production or are less effectively absorbed by all samples (Mohammed et al., 2024).

Fig. 10 illustrates the relationship between the mean free path (MFP) and photon energy for WO₃-NPs/PM composites containing different weight percentages of WO₃ nanoparticles (5%, 10%, 15%, and 20%). The mean free path (MFP) represents the average distance a photon travels within the material before interacting with it (via photoelectric absorption, Compton scattering, or pair production) (Basha et al., 2022). WO₃-NPs/PM-20 (highest concentration): Exhibits the shortest MFP values across the entire photon energy range, indicating the best photon attenuation efficiency. The high tungsten content significantly increases the probability of photon interactions due to tungsten's high atomic number and density (Akhdar H., 2025). At low photon energies (0–200 keV), the differences in MFP between the samples are relatively small but still significant. At intermediate photon energies (200–600 keV), the separation between the MFP curves becomes more pronounced. As photon energy increases, Compton scattering dominates, and materials with higher tungsten content continue to offer improved attenuation. At high photon energies (above 600 keV), the MFP increases rapidly for all samples, but the composites with higher WO₃ loading consistently maintain lower MFP values, indicating superior shielding even at higher energies.

4. Conclusions

WO₃-NPs/PM composites were successfully synthesized and demonstrated strong potential as effective, lightweight radiation

shielding materials. Structural analyses confirmed the retention of crystalline WO_3 and well-dispersed, plate-like nanostructures, while optical studies revealed stable UV absorption and tunable photoluminescence, dependent on nanoparticle concentration. FTIR analysis verified the chemical stability of the polymer-melanin matrix. Radiation shielding performance improved with increasing WO_3 content, particularly at low to intermediate photon energies, as indicated by reduced HVL and MFP values. The findings demonstrate that tungsten oxide nanoparticles act as efficient fillers within the Pluronic P123-melanin matrix (PM), offering lightweight, flexible, and lead-free radiation shielding appropriate for uses in medical imaging, nuclear reactors, and space exploration. Their performance diminishes at higher energies, meaning the need for improved nanoparticle dispersion and the integration of hybrid fillers. Subsequent investigations ought to concentrate on enhancing these characteristics for wider applicability, with further research needed to optimize mechanical properties and long-term durability for practical applications.

CRedit authorship contribution statement

Saad Aldawood: Writing–review & editing, supervision, project administration, investigation, funding acquisition **Hamoud Kassim & Aziz A Aziz:** Writing–original draft, methodology. **Syed Mansoor Ali, Ahmad A. Alsaleh, & Khalid Alzahrani:** Methodology, data curation.

Declaration of competing interest

The authors declare that they have no competing financial interests or personal relationships that could have influenced the work presented in this paper.

Declaration of generative AI and AI-assisted technologies in the writing process

The authors confirm that there was no use of Artificial Intelligence (AI)-Assisted Technology for assisting in the writing or editing of the manuscript and no images were manipulated using AI.

Acknowledgment

The authors are grateful to the Ongoing Research funding program (ORF-2025-328) at King Saud University, Riyadh, Saudi Arabia for supporting this research.

References

- Abbasova, N., Yüksel, Z., Abbasov, E., Gülbiçim, H., Tufan, M.Ç., 2019. Investigation of gammaray attenuation parameters of some materials used in dental applications. *Results Phys* 12, 2202-2205. <https://doi.org/10.1016/j.rinp.2019.02.068>
- Akhdar, H., 2025. Theoretical investigation of photon interaction and X-Ray imaging performance of PEEK-based composites for medical implants. *Polymers (Basel)* 17, 996. <https://doi.org/10.3390/polym17070996>
- Al-Ghamdi, H., Elsaifi, M., Sayyed, M.I., Almuqrin, A.H., Tamayo, P., 2022. Performance of newly developed concretes incorporating WO_3 and barite as radiation shielding material. *J Mater Res Technol* 19, 4103-4114. <https://doi.org/10.1016/j.jmrt.2022.06.145>
- Al-Hadeethi, Y., Sayyed, M.I., Rammah, Y.S., 2020. Fabrication, optical, structural and gamma radiation shielding characterizations of $\text{GeO}_2\text{-PbO-Al}_2\text{O}_3\text{-CaO}$ glasses. *Ceram Int* 46, 2055-2062. <https://doi.org/10.1016/j.ceramint.2019.09.185>
- Almoussa, N., Hassan, A.M., Issa, S.A.M., Obiedallah, F.M., Zakaly, H.M.H., 2024. Optimizing structural, morphological, optical, and photon attenuation properties of AZO nanocrystals for radiation shielding. *Opt Mater* 153, 115600. <https://doi.org/10.1016/j.optmat.2024.115600>
- Alsaif, N.A.M., Alfryyan, N., Al-Ghamdi, H., Abdelghany, A.M., Tharwat, M., Abouhaswa, A.S., Nabil, I.M., Rammah, Y.S., 2024. Influence of WO_3 replacement for CaO on physical, optical, and γ -ray protection properties of borotellurite glasses: A comparative study. *Ceram Int* 50, 32687-32698. <https://doi.org/10.1016/j.ceramint.2024.06.076>
- Basha, A., Levi, G., Amrani, T., Li, Y., Ankonina, G., Shekhter, P., Kornblum, L., Goldfarb, I., Kohn, A., 2022. Elastic and inelastic mean free paths for scattering of fast electrons in thin-film oxides. *Ultramicroscopy* 240, 113570. <https://doi.org/10.1016/j.ultramic.2022.113570>
- El-Zawawy, N.A., Kenawy, E.R., Ahmed, S., El-Sapagh, S., 2024. Bioproduction and optimization of newly characterized melanin pigment from *Streptomyces*

- djakartensis* NSS-3 with its anticancer, antimicrobial, and radioprotective properties. *Microb Cell Fact* 23, 23. <https://doi.org/10.1186/s12934-023-02276-y>
- Eren Belgin, E., Aycik, G.A., Kalemtaş, A., Pelit, A., Dilek, D.A., Kavak, M.T., 2015. Preparation and characterization of a novel ionizing electromagnetic radiation shielding material: Hematite filled polyester based composites. *Radiat Phys Chem* 115, 43-48. <https://doi.org/10.1016/j.radphyschem.2015.06.008>
- Fionov, A., Kraev, I., Yurkov, G., Solodilov, V., Zhukov, A., Surgay, A., Kuznetsova, I., Kolesov, V., 2022. Radio-absorbing materials based on polymer composites and their application to solving the problems of electromagnetic compatibility. *Polymers (Basel)* 14, 3026. <https://doi.org/10.3390/polym14153026>
- Giuliani, C., De Stefano, I., Mancuso, M., Fiaschini, N., Hein, L.A., Mirabile Gattia, D., Scatena, E., Zenobi, E., Del Gaudio, C., Galante, F., Felici, G., Rinaldi, A., 2024. Advanced electrospun composites based on polycaprolactone fibers loaded with micronized tungsten powders for radiation shielding. *Polymers (Basel)* 16, 2590. <https://doi.org/10.3390/polym16182590>
- Hannachi, E., Sayyed, M.I., Slimani, Y., Elsaifi, M., 2023. Structural, optical and radiation shielding peculiarities of strontium titanate ceramics mixed with tungsten nanowires: An experimental study. *Opt Mater* 135, 113317. <https://doi.org/10.1016/j.optmat.2022.113317>
- Hou, Y., Li, M., Gu, Y., Yang, Z., Li, R., Zhang, Z., 2018. Gamma ray shielding property of tungsten powder modified continuous basalt fiber reinforced epoxy matrix composites. *Polym Compos* 39. <https://doi.org/10.1002/pc.24469>
- Hsieh, S.S., Taguchi, K., 2024. Spectral information content of Compton scattering events in silicon photon counting detectors. *Med Phys* 51, 2386-2397. <https://doi.org/10.1002/mp.16990>
- Jamal AbuAlRoos, N., Azman, M.N., Baharul Amin, N.A., Zainon, R., 2020. Tungsten-based material as promising new lead-free gamma radiation shielding material in nuclear medicine. *Phys Med* 78, 48-57. <https://doi.org/10.1016/j.ejmp.2020.08.017>
- Kahraman, Z., Güngör, A., Buldu-Aktürk, M., Tan, M., Alp, E., Erdem, E., Genç, A., 2025. Phase-dependent optical, photocatalytic and capacitive properties of tungsten oxide nanowires. *Dalton Trans* 54, 7376-7390. <https://doi.org/10.1039/d4dt00212e>
- Khan, N., Mahajan, A., Arora, A., Sood, K., Kumari, S., Ghosh, S., Jha, M., 2024. Nanostructured tungsten trioxide developed from environmentally friendly green process as a promising cathode for excellent field emission. *Mater Chem Phys* 320, 129364. <https://doi.org/10.1016/j.matchemphys.2024.129364>
- Khattari, Z.Y., 2025. Tailoring structural and compositional influence on γ -ray shielding efficiency of Zeolite frameworks. *J Am Ceram Soc* 108. <https://doi.org/10.1111/jace.20560>
- Kim, S., Ahn, Y., Song, S.H., Lee, D., 2022. Tungsten nanoparticle anchoring on boron nitride nanosheet-based polymer nanocomposites for complex radiation shielding. *Compos Sci Technol* 221, 109353. <https://doi.org/10.1016/j.compscitech.2022.109353>
- Li, M., Feng, Y., Wang, J., 2023. Asymmetric conductive structure design for stabilized composites with absorption dominated ultra-efficient electromagnetic interference shielding performance. *Compos Sci Technol* 236, 110006. <https://doi.org/10.1016/j.compscitech.2023.110006>
- Menichetti, A., Mordini, D., Vicenzi, S., Montalti, M., 2024. Melanin for photoprotection and hair coloration in the emerging era of nanocosmetics. *Int J Mol Sci* 25, 5862. <https://doi.org/10.3390/ijms25115862>
- Mohammed, M.I., Yahia, I.S., Zahrn, H.Y., 2024. Radiation attenuation parameters of Ti_3SiC_2 MAX phase and their binary compounds using Phy-x/PSD software. *Mater Sci Semicond Process* 169, 107916. <https://doi.org/10.1016/j.mssp.2023.107916>
- Omana, L., Chandran, A., John, R.E., Wilson, R., George, K.C., Unnikrishnan, N.V., Varghese, S.S., George, G., Simon, S.M., Paul, I., 2022. Recent advances in polymer nanocomposites for electromagnetic interference shielding: A review. *ACS Omega* 7, 25921-25947. <https://doi.org/10.1021/acsomega.2c02504>
- Rayar, A., Naveen, C.S., Onkarappa, H.S., Betageri, V.S., Prasanna, G.D., 2023. EMI shielding applications of PANI-Ferrite nanocomposite materials: A review. *Synth Met* 295, 117338. <https://doi.org/10.1016/j.synthmet.2023.117338>
- Retailleau, C., Alaa Eddine, J., Ndagijimana, F., Haddad, F., Bayard, B., Sauviac, B., Alcouffe, P., Fumagalli, M., Bounor-Legaré, V., Serghéi, A., 2022. Universal behavior for electromagnetic interference shielding effectiveness of polymer based composite materials. *Compos Sci Technol* 221, 109351. <https://doi.org/10.1016/j.compscitech.2022.109351>
- Rotkovich, A.A., Tishkevich, D.I., Razanau, I.U., Vershinina, T.N., Bondaruk, A.A., German, S.A., Zubar, T.I., Sayyed, M.I., Dong, M., Yao, Y., Mahmoud, K.A., Silibin, M.V., Trukhanov, A.V., 2024. Development and study of lightweight recycled composite materials based on linear low-density polyethylene and W for radiation application. *J Mater Res Technol* 30, 1310-1318. <https://doi.org/10.1016/j.jmrt.2024.03.187>
- Sartoretto, T., McDermott, M.C., Stammen, L., Martens, B., Moser, L.J., Jost, G., Pietsch, H., Gutjahr, R., Nowak, T., Schmidt, B., Flohr, T.G., Wildberger, J.E., Alkadhi, H., 2024. Tungsten-based contrast agent for photon-counting detector CT angiography in calcified coronaries: Comparison to iodine in a cardiovascular phantom. *Invest Radiol* 59, 677-683. <https://doi.org/10.1097/RLI.0000000000001073>
- Sastry, D.N., Revanasiddappa, M., Suresh, T., Kiran, Y.T.R., Raghavendra, S.C., 2018. Electromagnetic shielding effectiveness studies on polyaniline/CSA- WO_3 composites at KU band frequencies. 2ND International conference on condensed matter and applied physics (ICC 2017) Bikaner, India, pp. 090067. <https://doi.org/10.1063/1.5032914>
- Sayyed, M., Hashim, S., Hannachi, E., Slimani, Y., Elsaifi, M., 2022. Effect of WO_3 nanoparticles on the radiative attenuation properties of SrTiO_3 perovskite ceramic. *Crystals* 12, 1602. <https://doi.org/10.3390/cryst12111602>
- Sayyed, M.I., Mhareb, M.H.A., Hamad, M.K., 2024. Physical, mechanical, and ionizing radiation shielding properties of $10\text{PbO-10Na}_2\text{O-(80-x)B}_2\text{O}_3\text{-xBaO}$ glasses. *Opt Mater* 150, 115237. <https://doi.org/10.1016/j.optmat.2024.115237>

- Shaaban, K.S., Alzahrani, A.S., Aloraini, D.A., Ismail, Y.A.M., 2024. RETRACTED: Radiation attenuation and optical behaviors of glass system: $21\text{SiO}_2-49\text{B}_2\text{O}_3-13\text{ZnO}-(17-x)\text{Na}_2\text{O}-x\text{WO}_3$. *Opt Mater* 148, 114852. <https://doi.org/10.1016/j.optmat.2024.114852>
- Shahapurkar, K., Gelaw, M., Tirth, V., Soudagar, M.E.M., Shahapurkar, P., Mujtaba, M.A., MC, K., Ahmed, G.M.S., 2022. Comprehensive review on polymer composites as electromagnetic interference shielding materials. *Polymers Polymer Composites* 30. <https://doi.org/10.1177/09673911221102127>
- Solak, B.B., Aktas, B., Yilmaz, D., Kalecik, S., Yalcin, S., Acikgoz, A., Demircan, G., 2024. Exploring the radiation shielding properties of B_2O_3 - PbO - TeO_2 - CeO_2 - WO_3 glasses: A comprehensive study on structural, mechanical, gamma, and neutron attenuation characteristics. *Mater Chem Phys* 312, 128672. <https://doi.org/10.1016/j.matchemphys.2023.128672>
- Sood, Y., Mudila, H., Chamoli, P., Saini, P., Kumar, A., 2024. Exploring the efficacy and future potential of polypyrrole/metal oxide nanocomposites for electromagnetic interference shielding: A review. *Mater Horiz* 11, 4256-4274. <https://doi.org/10.1039/d4mh00594e>
- Xie, W., Dhinojwala, A., Gianneschi, N.C., Shawkey, M.D., 2024. Interactions of melanin with electromagnetic radiation: from fundamentals to applications. *Chem Rev* 124, 7165-7213. <https://doi.org/10.1021/acs.chemrev.3c00858>
- Yao, Y., Sang, D., Zou, L., Wang, Q., Liu, C., 2021. A review on the properties and applications of WO_3 nanostructure-based optical and electronic devices. *Nanomaterials* 11, 2136. <https://doi.org/10.3390/nano11082136>
- Zamudio Diaz, D.F., Busch, L., Kröger, M., Klein, A.L., Lohan, S.B., Mewes, K.R., Vierkotten, L., Witzel, C., Rohn, S., Meinke, M.C., 2024. Significance of melanin distribution in the epidermis for the protective effect against UV light. *Sci Rep* 14, 3488. <https://doi.org/10.1038/s41598-024-53941-0>
- Zhou, S., Yang, Z., Feng, X., Zuo, J., Wang, N., Thummavichai, K., Zhu, Y., 2024. The frontier of tungsten oxide nanostructures in electronic applications. *iScience* 27, 109535. <https://doi.org/10.1016/j.isci.2024.109535>